An efficient solution to determine surface energy of powders and porous media: Application to untreated and treated lignin

Valentin Carretier, Monica Francesca Pucci, Clément Lacoste, Arnaud Regazzi, J. Lopez-Cuesta

An efficient solution to determine surface energy of powders and porous media: Application to untreated and treated lignin

Valentin Carretier [a], Monica Francesca Pucci [b,*], Clément Lacoste [a], Arnaud Regazzi [b], José-Marie Lopez-Cuesta [a]

[a] Polymers Composites and Hybrids (PCH), IMT Mines Ales, Ales, France
[b] LMGC, IMT Mines Ales, Univ Montpellier, CNRS, Ales, France

ARTICLE INFO

Keywords:
Capillary wicking
Lignin
Surface energy
Porous media

ABSTRACT

The estimation of solid surface energy is generally obtained through the determination of liquid/solid contact angles. Many questions arise in the literature about the appropriate contact angle to use (dynamic, quasi-static or static, measured at a macro or a micro-scale). Theoretically, equilibrium contact angles should be inserted into equations to determine surface energy components. However, for powders or porous materials more issues arise, notably due to the imbibition of the liquid into the medium. An apparent contact angle can be obtained using wicking tests and the modified Washburn equation. Nonetheless, Washburn hypotheses are not always respected or no longer valid during wicking meaning that this procedure could not allow to determine contact angles. This study has the aim to propose a new simple method to determine the surface energy components of powders and porous media. An experimental protocol coupled to a modified Jurin law is proposed. This protocol was applied to lignin particles used as reinforcement in polylactic acid (PLA). Some treatments were performed on lignin to improve the adhesion with PLA and the modifications due to the treatments were characterized. Reliable surface energy and components of untreated and treated lignin were obtained revealing the efficiency of the proposed method.

1. Introduction

Sustainable biocomposites have a growing interest in the polymer industry due to their interesting thermo-mechanical properties that are comparable to ones of conventional petroleum-derived composites. The use of both plant-derived biopolymers and biofillers with a biodegradable character is attractive for environmental reasons. Among the biopolymers, polylactic acid (PLA) has received wide commercial development in the recent past in many applications such as in biomedical [1] and packaging [2] materials. PLA is an aliphatic linear thermoplastic polyester derived from the fermentation of starch from agricultural crops [3] with an easy processability. However, several intrinsic properties of PLA such as brittleness, poor heat resistance and fire behavior still limit its industrial development. The addition of some biofillers like lignocellulosic biomass is an effective way to improve PLA properties and to extend its range of applications [4,5]. Lignin is one of the main structural components of lignocellulosic biomass and a very sought after resource in biocomposites field [6–8]. It is the second most abundant biopolymer on earth [9] and it is a by-product of the paper industry with a growing worldwide production [10]. As an amorphous copolymer, lignin is mainly composed of phenolic groups such as p-hydroxyphenyl (H-unit), guaiacyl (G unit) and syringyl (S Unit) that are residues from three monolignols (p-coumaryl, coniferyl and sinapyl alcohols) as lignin precursors [11,12]. Lignin, in powder form, has a wide set of applications as filler in composites, such as UV blocker [13–17], antioxidant [18–20], charring agent in flame retardancy [21–26], mechanical reinforcement [13,27,28] or surfactant [29–31]. However, the strong polar nature of lignin, due to the presence of hydroxyl groups, makes it incompatible with the non-polar PLA matrix, resulting in a poor interfacial filler-matrix adhesion [32]. Costes et al. [33], explained that the PLA is hydrolysed by lignin during processing.

Lignin chemical modification is then required to improve the interfacial adhesion between the filler and the polymer and then to improve the mechanical properties of PLA/lignin biocomposites. Multiple treatments are used for different issues, such as converting lignin into chemicals, fuels, or polymers [34]. Acetylation is a way to compatibilize

* Corresponding author.
E-mail address: monica.pucci@mines-ales.fr (M.F. Pucci).

https://doi.org/10.1016/j.apsusc.2021.152159

Table 1
Test liquids properties at 20 °C provided by suppliers, except values with standard deviation that were measured.

Solvant	ρ (g/cm^3)	η (mPa.s)	γ_L (mN/m)	γ^P (mN/m)	γ^D (mN/m)
n-Hexane	0.659	0.32	18.4	0.0	18.4
Water	0.998	1.00	72.8	51.0	21.8
Ethylene glycol	1.113	21.81	48.0	19.0	29.0
Lactic Acid	1.248	69.01 ± 1.01	42.2 ± 0.1	4.5 ± 0.4	37.7 ± 0.3

lignocellulosic materials with polyester [12,34]. It needs a reagent such as acid anhydrides or acidic compounds and a catalyst [35]. Moreover, esterification is a way to produce lignin-lactide copolymer [36]. Gordobil et al. [37] show that the incorporation of acetylated lignin increases the contact angle of a PLA/lignin composite and improves some mechanical properties such as the elongation at break. Phosphorylation of lignocellulosic biomass is an innovative and effective way to improve the fire behavior of biocomposites based on the addition of phosphorus [34], often present in fire retardants and more precisely in intumescent fire-retardant systems. Lignin is known as a charring agent combined with phosphorus fire retardants and it is also able to improve the thermal stability of polymers such as PLA [22,26]. However, to the best of our knowledge, there are actually no studies on the effects of phosphorylation on the matrix/lignin adhesion.

In this work, acetylation and phosphorylation treatments were performed on lignin and the surface properties of untreated and treated lignin were characterized. Thermogravimetric analysis (TGA), infrared spectroscopy (FTIR) characterizations and scanning electron microscopy (SEM) observations showed the effectiveness of both treatments on lignin. The enhancement of PLA/lignin thermal and mechanical properties is strongly related with the interfacial adhesion between fillers and PLA. To characterize this adhesion, the determination of the lignin and PLA surface energy is required. Surface energy is an intrinsic property of each liquid and solid material and, for a solid, it is obtained by means of equilibrium contact angle measurements. For PLA surface energy and its components, equilibrium contact angles are usually obtained using a sessile drop method, well-known in the literature [38]. However, in the case of fillers in form of powders or porous media such as lignin, some issues arise with this technique for measuring equilibrium contact angles, particularly due to the imbibition of liquids into the media [39–41]. Wicking tests are then performed as an alternative method, and they are described using the well-known modified Washburn equation for porous materials [39,42–45]. However this method, that theoretically allows the determination of apparent advancing contact angles [46,47], does not always give reliable results due to the Washburn hypotheses that are not respected or no longer valid [40,43,48]. A new simple method using a modified Jurin law for porous media and powder is proposed here in order to determine reliable apparent equilibrium contact angles. An experimental protocol based on capillary wicking and coupled to the modified Jurin law was set and applied to untreated and treated lignin. This approach was compared to the Washburn method. The obtained contact angles were then used in the Owens and Wendt equation to determine the surface energy and dispersive and polar components. Reliable surface energy and components of untreated and treated lignin were obtained revealing the efficiency of the proposed method. Lignins were then used as reinforcements for PLA. The biocomposites were observed by SEM to highlight the modification of adhesion at the filler/matrix interface due to the modification of fillers surface properties.

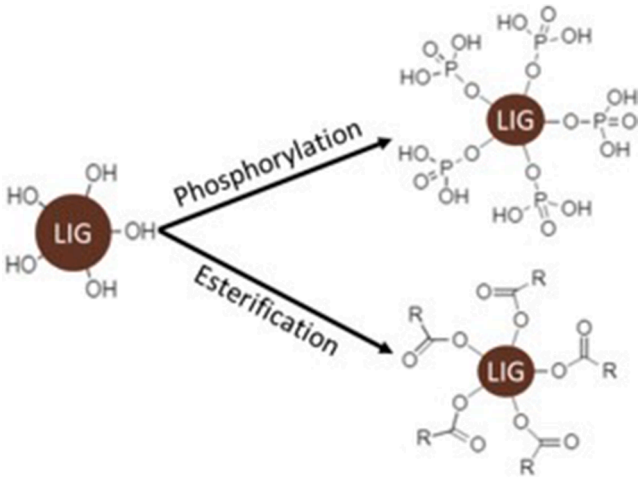

Fig. 1. Chemical treatments of lignin.

2. Material and method

2.1. Materials

The lignin used in this study is an alkali lignin supplied by TCI (Tokyo, Japan). This was named untreated or reference lignin (Ref-Lig). The content of methoxyl group is between 10 and 12 % and the median particle diameter is around 50 μm. For the lignin acetylation, the anhydride acetic (97% pure and supplied by Fisher chemical) and the methylimidazole (99% pure and supplied by Alfa Aesar) were used. For lignin phosphorylation, the *ortho*-phosphoric acid (85% pure and supplied by Panreac) and the urea (99.5% pure and supplied by Acros Organics) were used. The PLA Ingeo 2003D purchased from NatureWorks (USA) was used to manufacture biocomposite samples. For the surface energy determination, four liquids were tested with lignin. Table 1 shows density ρ, dynamic viscosity η, surface tension γ_L and dispersive γ^d and polar γ^p components for each liquid at standard conditions [49]. The n-hexane (99+ % pure and supplied by Chem-Lab) was used as totally wetting liquid. The water and the ethylene glycol (99.5 % pure and supplied by Chem-Lab) were used because of their polarity. The lactic acid (90 % pure, supplied by Sigma-Aldrich), was used expecting to have similar wetting properties of PLA. Dynamic viscosity of lactic acid was measured using a AR2000ex rheometer (TA Instrument) with a coaxial cylinder system. Surface tension and dispersive and polar components were determined using a K100SF tensiometer (Krüss) and performing a three-step procedure detailed in a previous work [50]. As expected, lactic acid was found to have a quasi-totally dispersive nature, with dispersive and polar components very close to ones of PLA [38].

2.2. Lignin treatment

A schematic representation of chemical treatments applied on lignin is given in Fig. 1. After both treatments, treated lignins were manually ground using an agate pestle and mortar set due to the agglomerates created during the chemical modifications.

2.2.1. Lignin acetylation

The treatment protocol was adapted from the literature [35]. A volume of 250 mL of acetic anhydride was introduced in a 500 mL round-bottomed flask and equilibrated at 65 °C with reflux. After that, 1 mL of 1-methylimidazole working as catalyst was added. A mass of 40 g of alkali lignin was added slowly in the flask. The mixture was equilibrated at 65 °C for 24 h. The reaction was stopped by introducing the mixture in 1.5 L of cold deionized water. Then the treated lignin was separated from the reaction mixture by centrifugation (Hettich, Rotina

Table 2
Biocomposites samples and lignins used.

Sample name	Lignin
A	untreated (Ref-Lig)
B	acetylated (Ac-Lig)
C	phosphorylated (P-Lig)

380). The lignin was washed from 3 to 5 times with deionized water in order to obtain a neutral pH (to remove acid residues). Then the lignin was dried in an oven at 80 °C for 24 h. The treated lignin was named acetylated lignin (or Ac-Lig).

2.2.2. Lignin phosphorylation

The treatment protocol was adapted from the literature [51–53] . A 60 % phosphoric acid was prepared using 85 % phosphoric acid and deionized water. The phosphoric acid was poured in a round-bottomed flask and stabilized at 80 °C with reflux. Then 12.5 g of urea were slowly added to the acid. The mixture was put under agitation. When the urea was fully dissolved, 25 g of alkali lignin were slowly added to the mixture under vigorous agitation. After 1 h of reaction the mixture was dried in an oven at 70 °C overnight, then it was heated at 150 °C during 2 h for the thermal curing. After that, the lignin was cooled at room temperature and washed with ethanol using centrifugation. Finally, the treated lignin was dried at 80 °C overnight. This lignin was named phosphorylated lignin (or P-Lig).

2.3. Biocomposites preparation

The biocomposites reinforced by untreated and treated lignin were prepared using a conical twin-screw micro-compounder (XPLORE, the Netherlands). The process conditions were the same for all samples. The temperature of mixing was 190 °C, the drain temperature was 180 °C. The screws rotational speed was set at 60 rpm and the mixing time was 3 min. The PLA and the lignin were vacuum dried at 60 °C before compounding. The ratio PLA/lignin was 4:1 by weight. Table 2 indicates the sample name and the lignin used for each biocomposite.

2.4. Lignin and biocomposites characterization

The characterization of thermal stability of the different lignins was performed using a Thermogravimetric Analysis (TGA) apparatus (SETSYS evolution, Setaram, France). Experiments were performed in the temperature range from 30 to 900 °C at the heating rate of 10 °C/min under nitrogen atmosphere (100 mL/min). The sample weight was approximately 12 mg.

The infrared spectroscopy of untreated and treated lignins was performed with a Fourier Transformation Infra-Red Attenuated Total Reflectance (FTIR-ATR) spectrometer (Vertex 70 FT MIR from Bruker, USA). The measurements were performed in transmission mode using lignin-KBr compressed pads. Sample pads were composed of 150 mg of KBr and 5 mg of lignin, that were ground together and compressed. The resolution was 4 cm^{-1}. 32 scans for the background and 32 scans for the spectra acquisition were conducted. The spectral range was from 4000 cm^{-1} to 400 cm^{-1} and it was analyzed with the OPUS software, provided with the spectrometer.

The phosphorus analysis was also performed using an Inductively Coupled Plasma Optical Emission Spectrometry (ICP-OES) with an Activa M apparatus from Horiba. The phosphorus peak detection wavelength is 213.618 nm. The mineralization of the sample was made using a microwave MLS 1200 Mega from Milestone.

A Scanning Electron Microscopy (SEM) Quanta 200 FEG (FEI Company, USA) in environmental mode equipped with an X-Max 80 N SDD detector was used to observe lignins and biocomposites, as well as for the elementary composition analysis of lignins. The voltage use for the sample was 3 kV and the spot size was 3.0. For the observations of biocomposites, the sample surfaces were prepared using a cryo-ultramicrotome (EM UC7, Leica).

The densities of different lignins were measured using a helium AccuPyc 1330 pycnometer (Micromeritics). Three measurements were carried out for each sample.

2.5. Lignin surface energy determination

2.5.1. Theoretical aspects

In this section the well-known Washburn approach derived from the capillary rise in a tube and applied to porous media is described. Based on this approach, the Jurin law and an extension of this law for porous media are presented. Hypotheses and assumptions in order to obtain reliable contact angles are given. The Owens and Wendt equation using contact angles to determine surface energy and components is also presented here.

When the hypothesis of a visco-capillary regime is valid [54], the Washburn equation (Eq. (1)) describing the capillary rise of a liquid in a tube can be written as follows:

$$h^2(t) = \frac{r \cdot \gamma_L \cdot cos\theta_a \cdot t}{2 \cdot \eta} \tag{1}$$

where h is the height travelled by the liquid front, r is the radius of the capillary tube, γ_L is the liquid surface tension, θ_a is the advancing contact angle, η is the liquid viscosity and t is the time of flow.

The capillary rise is stopped when the capillary force is balanced by the liquid weight in the tube. From this equilibrium, the Jurin law (Eq. (2)) is obtained:

$$h_{eq} = \frac{2 \cdot \gamma_L \cdot \cos(\theta e)}{r \cdot \rho \cdot g} \tag{2}$$

where h_{eq} is the equilibrium height of liquid column, g is the gravitational acceleration and θ_e is the equilibrium contact angle.

The Washburn equation can be expressed as a function of the mass gained during the liquid rise and it has been modified for powders or porous media packed in a cylindrical column [44] (Eq. (3)):

$$m(t)^2 = \left[\frac{(c\bar{r}) \cdot \varepsilon \cdot (\pi R^2)^2}{2}\right] \frac{\rho^2 \cdot \gamma_L \cdot cos\theta_a}{\eta} t \tag{3}$$

where assuming the porous medium as a capillary tube arrangement, c is a parameter inversely proportional to the tortuosity and $\bar{r}$ is the mean capillary radius. The c $\bar{r}$ is defined as a geometric factor. R is the inner radius of the column (or the cylindrical sample holder), ε is the porosity of the medium and θ_a is the apparent advancing contact angle, representative of the interaction between the liquid and the porous medium during the capillary rise.

Following the same approach used for Washburn equation, an extension of Jurin law for porous media packed in a column is proposed here. The Jurin law (Eq. (2)), is expressed as a function of the liquid mass at the equilibrium (m_{eq}) and modified for powders or porous media packed in a cylindrical sample holder (Eq. (4)):

$$m_{eq} = \frac{2 \cdot \gamma_L \cdot \cos(\theta e)}{(c\bar{r}) \cdot g} \varepsilon \cdot (\pi R^2) \tag{4}$$

where θ_e is now an apparent equilibrium contact angle, representative of the liquid/porous medium interaction at equilibrium. It is important to point out that the proposed approach has not the aim to predict the equilibrium meniscus shape [55,56] because of the irregular three-dimensional morphology of used porous media. The benefit and the originality of using this approach consist in taking advantage of the recorded equilibrium mass achieved after capillary wicking to obtain an apparent equilibrium contact angle, representative of the liquid/porous medium interaction at equilibrium.

It is well-known that the surface energy of a solid (γ_S) can be defined

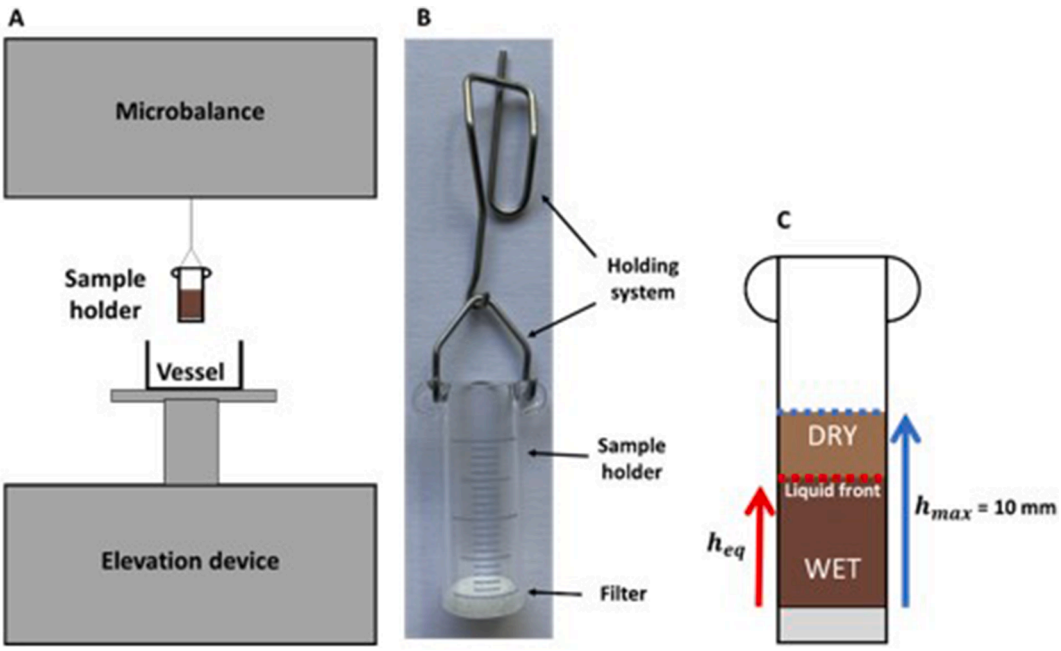

Fig. 2. A) Tensiometer, B) sample holder system, C) Wicking representation with dry and wet lignin.

as the sum of two components: a dispersive component (γ_S^d) and a polar component (γ_S^p) (Eq. (5)):

$$\gamma_S = \gamma_S^d + \gamma_S^p \tag{5}$$

Using at least two test liquids with known surface tensions (γ_L) and components (γ_L^d, γ_L^p) for contact angle measurements, the dispersive and polar components of solid surface energy can be determined with the Owens-Wendt equation (Eq. (6)):

$$\gamma_S + \gamma_L - \gamma_{SL} = 2\left(\gamma_S^d \gamma_L^d\right)^{0.5} + 2\left(\gamma_s^p \gamma_L^p\right)^{0.5} \tag{6}$$

where γ_{SL} is the liquid/solid interfacial tension. Incorporating the Young-Laplace equilibrium equation in the Eq. (6) the equilibrium contact angle appears, as follows:

$$\gamma_L(1+\cos\theta_e) = 2\left(\gamma_S^d \gamma_L^d\right)^{0.5} + 2\left(\gamma_s^p \gamma_L^p\right)^{0.5} \tag{7}$$

Using more than two liquids with known surface tensions and components for equilibrium contact angles measurements, a linear form of Eq. (7) can be used to determine the solid surface energy and components:

$$\frac{\gamma_L(1+\cos\theta_e)}{2\left(\gamma_L^d\right)^{0.5}} = \left(\gamma_s^p\right)^{0.5}\frac{\left(\gamma_L^p\right)^{0.5}}{\left(\gamma_L^d\right)^{0.5}} + \left(\gamma_s^d\right)^{0.5} \tag{8}$$

It is important to point out that for surface energy determination, equilibrium contact angles are defined in Eq. (7) and Eq. (8), might be significantly different from the advancing contact angles [57]. Therefore, for porous materials, using the apparent equilibrium contact angles obtained by the modified Jurin law could be an efficient solution to determine reliable surface energy and components.

2.5.2. *Experimental aspects*

The dynamic test of capillary wicking was carried out using a K100SF tensiometer (Krüss, Germany). The K100SF is provided with an electronic microbalance (resolution of 10^{-7} g) where the sample holder containing the porous medium is clamped (Fig. 2A). The sample holder consists of a hollow cylinder with an inner radius of 4.6 mm and a graduated height of 20 mm (Fig. 2B). The samples were prepared in the same conditions. The sample holder was firstly washed with distilled water and secondly with acetone using sonication during 2 min. When

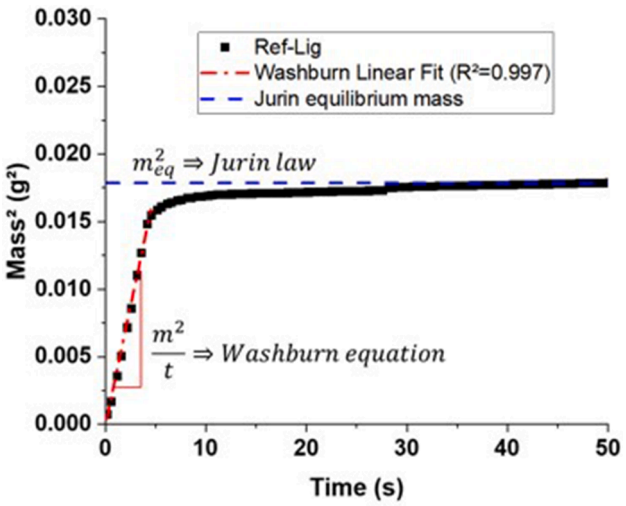

Fig. 3. Washburn linear fit of experimental test of reference lignin with n-hexane and Jurin squared equilibrium mass.

the sample holder was dried, a paper filter was added. Then the lignin was inserted in the sample holder in order to achieve a filled height of 10 mm. Knowing the density of each type of lignin (measured by the pycnometer) and the sample-holder volume that had to be filled, the lignin mass was determined in order to set the same powder volume fraction V_p for each test and lignin. A V_p of 45% (resulting in a porosity of 55%) was then chosen for all wicking tests.

Wicking tests were carried out with reference, acetylated and phosphorylated lignins using n-hexane, water, ethylene glycol and lactic acid. All tests were performed in standard conditions. Both modified Washburn equation (Eq. (3)) and Jurin law (Eq. (4)) were applied for these experiments in order to characterize the c $\bar{r}$ and the contact angles corresponding to each theory.

Once the sample holder is clamped to the tensiometer, the vessel is moved. The liquid vessel rises at a speed of 0.5 mm/s up to detect the bottom surface of sample holder. At this moment the spontaneous capillary wicking of liquid into the porous medium occurs and the

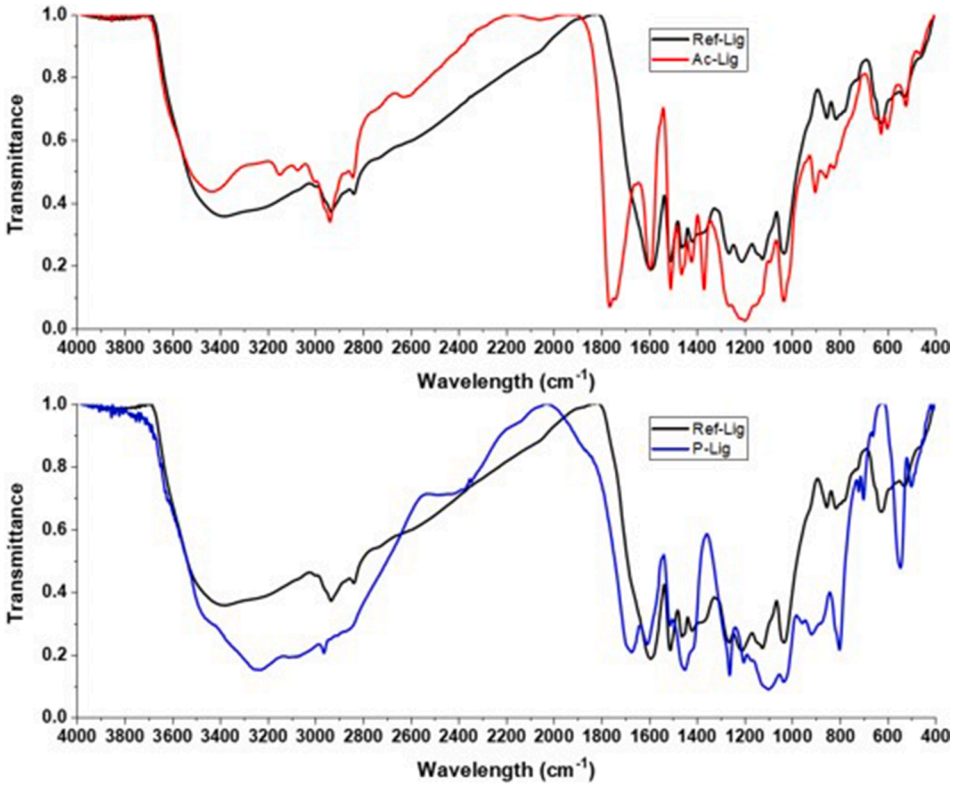

Fig. 4. FTIR transmission spectra of untreated and treated lignin.

tensiometer records the squared mass gain as a function of time (m^2 vs t). An example of experimental curve is given in Fig. 3 for the reference lignin with n-hexane. The Washburn equation is verified if the curves recorded by the tensiometer during capillary wicking (m^2 vs t) have a linear trend. Firstly, n-hexane is used as totally wetting test liquid ($\cos\theta$ is approximated to 1) which allows the determination of $c\,\bar{r}$ from fit of the experimental wicking curve (m^2 vs t) with Eq. (3). Fig. 3 shows the Washburn linear fit on the experimental wicking curve for the reference lignin with n-hexane. In the same way, once $c\,\bar{r}$ is known, the linear fit of wicking curve with other liquids can be used to determine the apparent advancing contact angles according to Eq. (9). However, these equations are valid and the method is applicable only if experimental curves have a linear trend. More details about Washburn theory and experiences are given in [39,43,58].

$$c\bar{r} = 2\left(\frac{m^2}{t}\right)\frac{\eta}{\rho^2\cdot\gamma_L\cdot\varepsilon\cdot(\pi R^2)^2} \; and \; \theta_a = cos^{-1}\left(2\left(\frac{m^2}{t}\right)\frac{\eta}{(c\bar{r})\cdot\rho^2\cdot\gamma_L\cdot\varepsilon\cdot(\pi R^2)^2}\right) \tag{9}$$

It is now interesting to observe that the curve (Fig. 3) reaches an equilibrium weight (m_{eq}) due to the saturation of the porous medium by the test liquid. To apply the Jurin law this equilibrium mass can be used. Two cases can occur:

(a) the equilibrium weight is obtained at a height inferior to the top of powder ($h_{eq} < 10$ mm, Fig. 2C) with the observation of a certain amount of dried powder at the top of the sample. This configuration occurred for most of the tests.
(b) the powder is totally wetted and the equilibrium weight is then forced at the top of the sample ($h_{eq} = 10$ mm). This occurred for n-hexane, being a totally wetting liquid. In this case an angle of 0° is assumed.

As for the Washburn approach, also for the Jurin law application, the squared equilibrium mass (m_{eq}^2) obtained with n-hexane was used for the calculation of the $c\,\bar{r}$, according to Eq. (4) and assuming an apparent equilibrium contact angle of 0° (Fig. 3). Afterwards, the m_{eq}^2 obtained with the other test liquids were used to determine the apparent equilibrium contact angles, according to Eq. (10):

$$c\bar{r} = \frac{2\cdot\gamma_L\cdot\varepsilon\pi\cdot R^2}{g\cdot m_{eq}} \; and \; \theta_e = cos^{-1}\frac{m_{eq}\cdot c\bar{r}\cdot g}{2\cdot\gamma_L\cdot\varepsilon\cdot\pi\cdot R^2} \tag{10}$$

It is important to note that, even if the Washburn hypotheses are not valid, the new Jurin approach described here will be applicable and an equilibrium contact angle will be identified, since one of the two cases *a* and *b* always occurs.

3. Results and discussion

3.1. Lignin treatments characterization

The lignin treatments were firstly characterized to assess their effects on the physico-chemical properties of the lignin. Infrared analysis, TGA and EDX results indicate if the treatment is effective and if it has an effect on the thermal stability of the lignin.

Infrared transmission spectra of the untreated and treated lignins are presented in Fig. 4 and they are in good agreement with literature data [59]. A large band between 3250 cm^{-1} and 3500 cm^{-1} corresponds to O—H stretching, due to the presence of hydroxyl groups. The two bands at 1591 and 1508 cm^{-1} are corresponding to the vibration of the C═C bonds of the aromatic skeleton, and 1420 cm^{-1} is corresponding to the C—H aromatic ring vibrations. Those bands are obtained in all spectra indicating that the different treatments do not alter the aromatic skeleton of the lignin. Acetylated lignin (Fig. 4 in red) presents a reduction of the O—H stretch band and the intensity of the CH3— and CH2— is increased. The esterification results in a reaction with the hydroxyl groups leading to the formation of an alkanoate chain. At 1766 and 1735 cm^{-1} two bands, respectively corresponding to an ester C═O bond stretch and a ketone C═O bond stretch significantly increased. As found

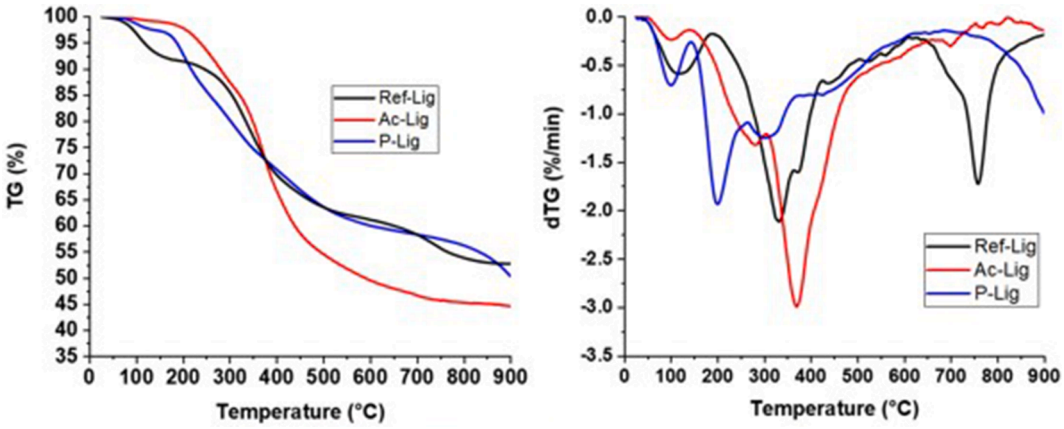

Fig. 5. TG and dTG curves of untreated and treated lignins.

Table 3
TGA results for the different lignins.

Samples	$T_{on\text{-}set}$ °C	Residue Mass %
Ref-Lig	288	53
Ac-Lig	245	44
P-Lig	202	49

Table 4
Elementary composition of lignins.

Lignin	Elementary composition (wt%)					
	C	O	S	Na	P	N
Ref-Lig	57.1 ± 0.2	32 ± 0.2	4.4 ± 0.0	6.2 ± 0.1	–	–
Ac-Lig	66.9 ± 0.1	29.7 ± 0.2	2.6 ± 0.1	0.5 ± 0	–	–
P-Lig	36 ± 2.2	38.4 ± 1.0	1.7 ± 0.1	0.5 ± 2	13.8 ± 0.9	8.6 ± 0.5

by Fox et al. [35], a cluster of bands between 1150 and 1270 cm^{-1} was observed. It is linked to the stretches of few bonds as C—C, C—O and C═O. This is therefore consistent with lignin acetylation.

The phosphorylation aimed at the addition of phosphorus to the lignin macromolecule and, as seen in the Fig. 1, phosphorylation route adds two hydroxyls sites for one grafted phosphoric compound. FTIR spectra of phosphorylated and untreated lignin are shown in Fig. 4, respectively in blue and black. Some bands between 3300 and 3600 cm^{-1}, attributed to the N—H and N—H_2 bonds, appeared in the same wavelength range as the hydroxyl groups. It could then explain that the transmittance of the band in those wavelengths did not decrease. On the P-Lig spectra, the large bands attributed to OH stretching were also more intense than Ref-Lig. This could be due to the OH added with the phosphorylation and the presence of urea. Moreover, P-Lig presents at 1668 cm^{-1} a band corresponding to the C═O bond of the urea. This could indicate that: (i) the washing step was insufficient to eliminate unreacted urea or (ii) C═O bonds between hydroxyl groups and carbon atoms of urea were formed, as reported by Ji et al. [52]. An additional peak observed at 1103 cm^{-1} in P-Lig and not present in the reference lignin was attributed to the stretch of P═O(OH) bond. This bond is present in the phosphoric acid and probably in the phosphorylated lignin. At 918 cm^{-1}, a peak appeared which can either belong to the P—O bond of P═O(OH) group or to the P—O—C bond of a P—O-aromatic structure. Peaks at 804 cm^{-1} and 544 cm^{-1} are attributed to the urea. P-Lig seems to contain phosphorus that reacted and cross-linked to the lignin hydroxyl groups.

Thermogravimetric analyses of all lignins are shown in Fig. 5 and the obtained results are detailed in Table 3. A thermal degradation in three steps was observed for the reference lignin. At 106 °C the evaporation of water physically adsorbed by lignin occurs. At this step, lignin is not thermally damaged, but it is dried. The temperature of initial degradation ($T_{on\text{-}set}$) is around 288 °C for the reference lignin. Between 300 °C and 400 °C, a degradation of the linkage between lignin monomeric units such as the linkages β-β and C-C [39] with a maximal loss of −1.95 %/min is observed. Between 700 and 800 °C the degradation of the carbon backbone of the lignin occurs [39]. The char residue obtained for the reference lignin is around 53 wt% (Table 3).

The acetylated lignin is dehydrated at 100 °C as seen with the dTG curve. However, the amount of evaporated water is significantly lower than for the reference lignin. The linkage degradation appears later than the alkali lignin with a peak of mass loss at 372 °C. However, the mass loss rate is drastically higher at −2.98 %/min. The reason is probably that the acetylation is adding more C-C linkage that are thermally degraded. Moreover, the degradation of the carbon backbone is less significant here than for the reference lignin. At 900 °C the char residue is 44 wt%. The acetylated lignin $T_{on\text{-}set}$ is 245 °C that is lower than for the Ref-Lig. Gordobil et al. [37] found that the $T_{on\text{-}set}$ of acetylated lignin is higher (266 °C) than the commercial lignin (259 °C). This could be attributed to the difference of the lignin source and of the protocol of chemical treatment. However, the char residue for the acetylated lignin is 44%, which is also lower than the reference lignin. This value is consistent with those found in the literature [37]. The degradation around 200 °C is attributed to some residues of urea [52]. The first degradation step on Ac-Lignin is attributed to the chemical treatment. The chemical treatment adds some linkages able to degrade or catalyst the degradation of other linkages.

Phosphorylated lignin presents a dehydration around 100 °C. $T_{on\text{-}set}$ was 202 °C. The mass residue was 49 wt% at 900 °C. P-Lig shows a first step of degradation at 198 °C and a second step between 270 °C and 340 °C. Prieur et al. [60] assumed that in the case of phosphorylated lignin, this degradation step is due to the dehydration of the lignin that is catalyzed by phosphorus-based chemicals. This third step could be due to the degradation of the lignin linkages. From P-Lig dTG curve it is possible to observe a fourth degradation step that occurred from 760 °C, which could be attributed to the lignin carbon backbone degradation that is delayed in comparison to the reference lignin.

TGA and FTIR analysis showed that the esterification protocol applied for lignin acetylation was effective. TGA shows that the acetylated and the phosphorylated lignins are less stable due to the chemical treatment. Phosphoric acid and urea are present with lignin as seen in the FTIR spectra and the TGA since urea degradation seems noticeable around 200 °C. TGA shows that the phosphorylated lignin is improving the char formation during a thermal degradation under N_2. It is also

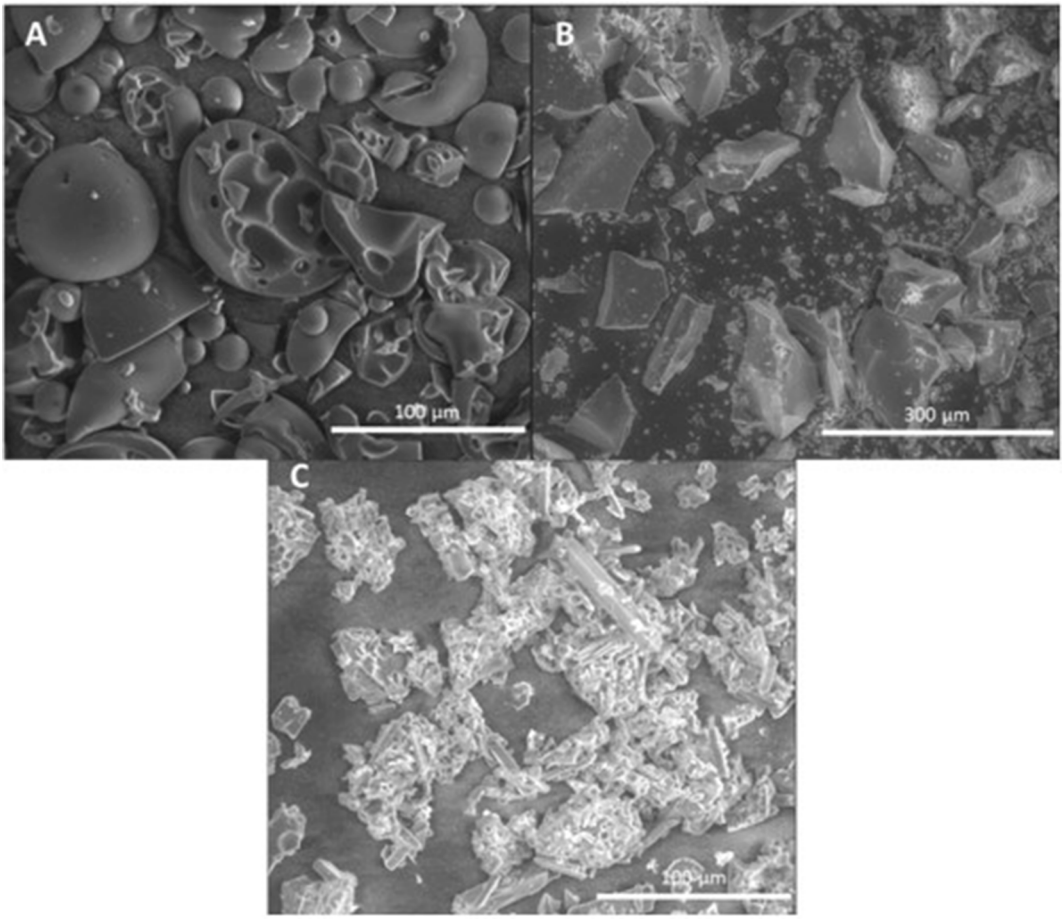

Fig. 6. SEM pictures of the lignin (A) Ref-Lig, (B) Ac-Lig and (C) P-Lig.

Table 5
Density of lignins.

Lignin	Density g/cm^3
Ref-Lig	1.409 ± 0.001
Ac-Lig	1.350 ± 0.002
P-Lig	1.562 ± 0.006

confirmed that the P-Lig is bringing phosphorus, which could be useful for the thermal stability of the biocomposite.

Results of EDX analysis are shown in Table 4 for all lignins. An increase of the carbon content is observed for the Ac-Lig. This is due to the esterification of the lignin that is adding carbon source. Moreover, the esterification process seems to reduce the content of Na and S. P-Lig has nitrogen in its elementary composition due to the residues of urea, which is consistent with the results of FTIR spectra and TGA curves. P-Lig contains more oxygen that can be related to P═$(OH)_n$ bonds. The phosphorylation process removes a significant part of Na and a small part of S.

SEM pictures in Fig. 6 show that the treatments on lignin modify the morphological aspect of Ref-Lig. Lignin of reference has a nodular shape. The treatments seem to dissolve a part of lignin and precipitate at the end of process. Ac-Lig exhibits an angular shape due to the grinding step. P-Lig presents a more different morphology, due to the precipitation of lignin and the presence of urea crystals, recognizable by their needle shape. The presence of these urea needles could have an effect on the surface area analysis and particularly on the determination of c $\bar{r}$. In Table 5, results of measured density for all lignin are given. Acetylation reduces lignin density, maybe due to the creation of porosity, while P-Lig shows a higher density.

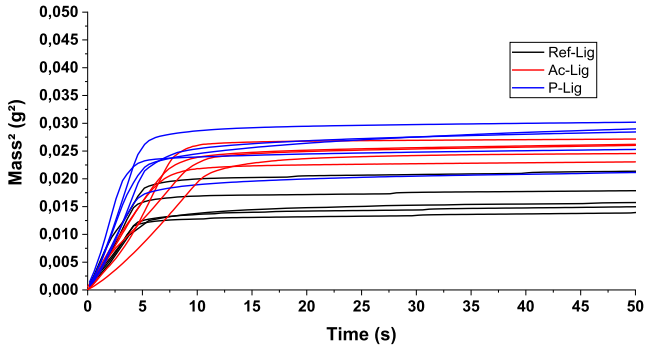

Fig. 7. Wicking curves with n-hexane for Ref-Lig, Ac-Lig, P-Lig.

3.1.1. *Characterization of c$\bar{r}$ and θ*

In this section, the results of capillary wicking tests on the different lignins with the test liquids are described. As previously mentioned, five tests were firstly performed with n-hexane (Fig. 7) in order to determine the c $\bar{r}$ for each lignin. It is possible to observe that the curves show a rapid wicking (less than 10 s) for untreated and treated lignins. All the samples were fully wetted showing a linear trend of wicking and the squared equilibrium mass was in a range between 0.0125 and 0.030 g^2 for all lignins. The slope of the curve (m^2/t) and the equilibrium mass (m_{eq}) were then used for the respective calculation of c $\bar{r}$ based on Washburn and Jurin equations. As shown in Table 6, the Washburn c $\bar{r}$ are different following the treatment. However, the c $\bar{r}$ of Ac-Lig is quite

Table 6
Results of geometric factors obtained by the Washburn theory and the Jurin law.

Samples	Washburn				Jurin		
	m^2/t (g^2/s)	R^2	$c\bar{r}$ m	Mean $c\bar{r}$ m	m_{eq}^2 (g^2)	$C\bar{r}$ (m)	Mean $c\bar{r}$ (m)
	Linear fit from 0 to 5.6 s				Mass^2 at end of recording		
Ref-Lig 1	0.00227	0.9862	1.386E−07	1.779E−07 ± 3.37E−08	0.01574	0.001093213	0.001068 ± 8.74E−05
Ref-Lig 2	0.00347	0.9926	2.118E−07		0.02136	0.00093844	
Ref-Lig 3	0.00267	0.9975	1.629E−07		0.01396	0.001160819	
Ref-Lig 4	0.00352	0.9968	2.149E−07		0.01786	0.001026281	
Ref-Lig 5	0.00265	0.9995	1.618E−07		0.01497	0.001120976	
	Linear fit from 0 to 8 s				Mass^2 at end of recording		
Ac-Lig 1	0.00232	0.9946	1.416E−07	1.647E−07 ± 3.56E−08	0.02963	0.000796785	0.0008334 ± 3.78E−05
Ac-Lig 2	0.00292	0.9969	1.782E−07		0.02979	0.000794642	
Ac-Lig 3	0.00187	0.9939	1.141E−07		0.02455	0.000875349	
Ac-Lig 4	0.0032	0.9982	1.953E−07		0.02503	0.000866915	
Ac-Lig 5	0.00318	0.9871	1.941E−07		0.02716	0.000832228	
	Linear fit from 0 to 5.2 s				Mass^2 at end of recording		
P-Lig 1	0.00451	0.9917	2.753E−07	2.942E−07 ± 4.26E−08	0.02899	0.000805532	0.0008428 ± 6.25E−05
P-Lig 2	0.00433	0.9924	2.643E−07		0.02844	0.000813284	
P-Lig 3	0.00562	0.9838	3.430E−07		0.02529	0.000862447	
P-Lig 4	0.00373	0.9975	2.277E−07		0.02113	0.000943533	
P-Lig 5	0.0536	0.9958	3.272E−06		0.03019	0.000789361	

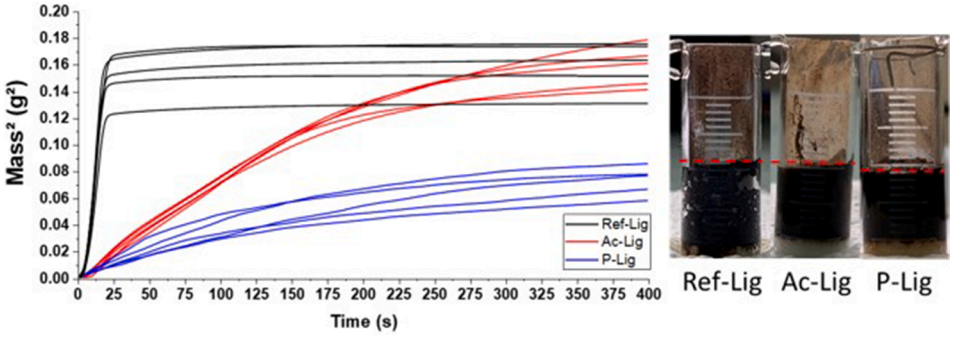

Fig. 8. Wicking curves with water for Ref-Lig, Ac-Lig, P-Lig and liquid equilibrium height (dash line in red). (For interpretation of the references to colour in this figure legend, the reader is referred to the web version of this article.)

Table 7
Results of wicking with water obtained by the Washburn equation and the Jurin law.

Samples	Washburn				Jurin		
	m^2/t (g^2/s)	R^2	θ_a (°)	$\bar{\theta}_a$ (°)	m_{eq}^2 (g^2)	θ_e (°)	$\bar{\theta}_e$ (°)
	Linear fit from 0 to 10 s				Mass^2 at 400 s		
Ref-Lig-1	0.0127	0.995	–	–	0.175	34.52	38.29 ± 4.19
Ref-Lig-2	0.0117	0.998	–		0.174	34.87	
Ref-Lig-3	0.0140	0.999	–		0.152	39.93	
Ref-Lig-4	0.0116	0.997	–		0.163	37.45	
Ref-Lig-5	0.00935	0.998	–		0.131	44.68	
	Linear fit from 0 to 180 s				Mass^2 at 400 s		
Ac-Lig-1	0.000675	0.992	85.14	85.13 ± 0.24	0.179	49.52	52.29 ± 2.13
Ac-Lig-2	0.000691	0.996	85.02		0.161	51.95	
Ac-Lig-3	0.000633	0.990	85.44		0.146	54.08	
Ac-Lig-4	0.000696	0.996	84.98		0.141	54.72	
Ac-Lig-5	0.000686	0.995	85.06		0.167	51.17	
	Linear fit from 0 to 110 s				Mass^2 at 400 s		
P-Lig-1	0.000462	0.973	88.14	88.57 ± 0.32	0.0778	64.33	65.23 ± 1.98
P-Lig-2	0.000275	0.992	88.89		0.0581	68.02	
P-Lig-3	0.000414	0.996	88.33		0.0858	62.95	
P-Lig-4	0.000296	0.997	88.81		0.0769	64.49	
P-Lig-5	0.000330	0.987	88.67		0.0667	66.36	

similar to the c $\bar{r}$ of Ref-Lig, while the c $\bar{r}$ of P-Lig is significantly different. This seems to be consistent with the change of morphology of treated lignins (observed in Fig. 6). Assuming that the mean porous radius was the same for these tests, since the same V_p was set, the change of morphology should mainly affect the tortuosity of media and then the c parameter. Concerning the c $\bar{r}$ obtained by the Jurin law, they were found quite similar. In this case the c $\bar{r}$ derives from an equilibrium mass, then it does not consider the morphology and the tortuosity of media in

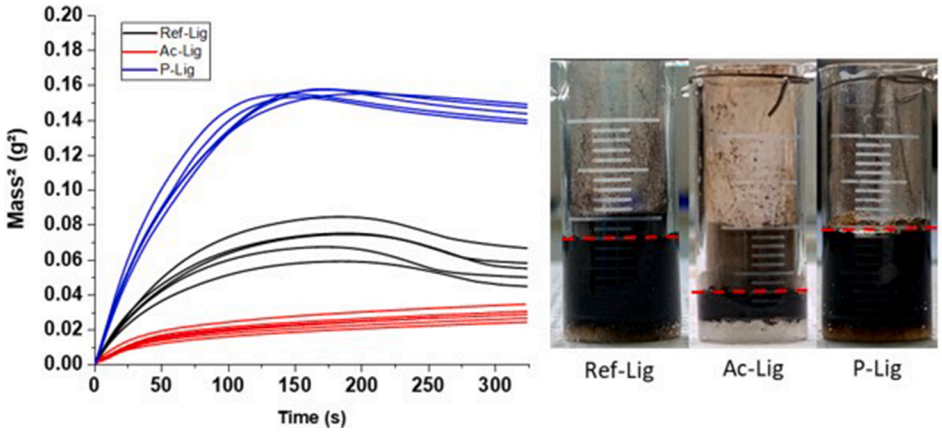

Fig. 9. Wicking curves with ethylene glycol for Ref-Lig, Ac-Lig, P-Lig and liquid equilibrium height (dash line in red). (For interpretation of the references to colour in this figure legend, the reader is referred to the web version of this article.)

Table 8
Results of wicking with ethylene glycol obtained by the Jurin law.

Samples	Jurin		
	m_{eq}^2 (g^2)	θ_e (°)	$\overline{\theta}_e$ (°)
	Mass² at 325 s		
Ref-Lig-1	0.0578	44.14	45.78 ± 4.26
Ref-Lig-2	0.0497	48.31	
Ref-Lig-3	0.0547	45.72	
Ref-Lig-4	0.0664	39.73	
Ref-Lig-5	0.0445	50.99	
	Mass² at 325 s		
Ac-Lig-1	0.0240	68.83	67.52 ± 1.02
Ac-Lig-2	0.0262	67.85	
Ac-Lig-3	0.0262	67.84	
Ac-Lig-4	0.0301	66.17	
Ac-Lig-5	0.0283	66.91	
	Mass² at 325 s		
P-Lig-1	0.147	25.41	26.8 ± 1.83
P-Lig-2	0.138	28.96	
P-Lig-3	0.144	26.83	
P-Lig-4	0.149	24.64	
P-Lig-5	0.140	28.26	

the same way, but it considers the liquid saturation of samples, that was similar with n-hexane.

Using the respective c $\overline{r}$, the determination of the contact angles was made applying both Washburn and Jurin approaches with the other test liquids, according to the experimental procedure.

Fig. 8 shows wicking curves obtained for all lignins with water. A photo of one sample per lignin after the test is given to show the height reached by the liquid at the equilibrium. Table 7 shows the results of contact angles obtained with water from the Washburn equation (Eq. (3)) and the Jurin law (Eq. (4)). One can observe that Ref-Lig was almost fully wetted by water with a fast wicking. A linear trend of m^2 vs t was found and the obtained cosines of θ_a were superior or equal to 1 for all tests, suggesting a total wetting ($\theta_a \approx 0°$). Concerning the treated lignins, the wicking kinetics were slower and a linear trend was not found for the entire wicking curve, but up to respectively 180 s for Ac-Lig and 110 s for P-Lig. Considering these fits and the geometric factors, similar apparent advancing contact angles were found for Ac-Lig (85.13 ± 0.24°) and P-Lig (88.57 ± 0.32°). Contact angles were then calculated considering the squared mass reached at the equilibrium and applying the modified Jurin law (Eq. (4)). In this case, the geometric factors obtained with the same theory were used. For Ref-Lig and Ac-Lig that had similar equilibrium mass, the contact angles were found to be 38.29 ± 4.19° and 52.29 ± 2.13° respectively. The P-Lig showed a lower equilibrium mass of water, that was consistent with observed equilibrium height, and the apparent equilibrium contact angle was higher (65.23 ± 1.98°).

Fig. 9 shows wicking curves obtained for all lignins with ethylene glycol and photos of one sample per lignin after the test. One can observe that wicking kinetics were very different as a function of lignin. However, no curves showed a linear trend and then the Washburn equation could not be applied to determine the advancing contact angles. The

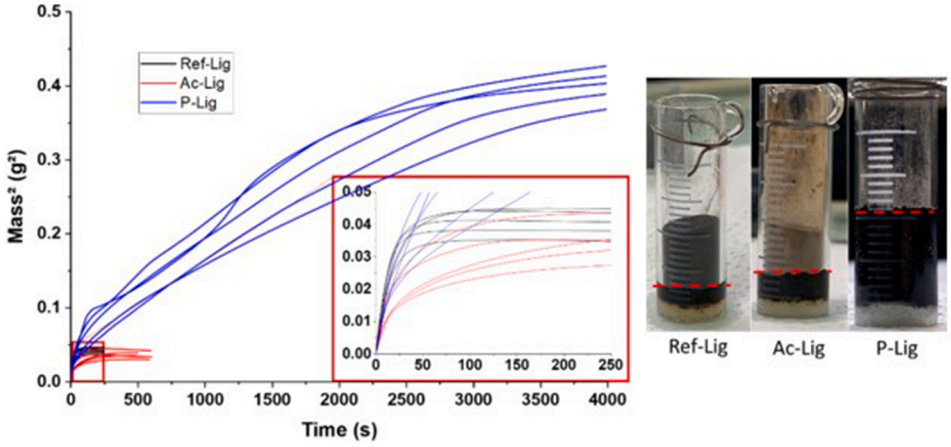

Fig. 10. Wicking curves with lactic acid for Ref-Lig, Ac-Lig, P-Lig and liquid equilibrium height (dash line in red). (For interpretation of the references to colour in this figure legend, the reader is referred to the web version of this article.)

Table 9
Results of wicking with lactic acid obtained by the Jurin law.

Samples	Jurin		
	m_{eq}^2 (g^2)	θ_e (°)	$\overline{\theta}_e$ (°)
	Mass^2 at the end of recording		
Ref-Lig-1	0.0436	44.83	46.95 ± 2.66
Ref-Lig-2	0.0448	44.06	
Ref-Lig-3	0.0407	46.77	
Ref-Lig-4	0.0351	50.52	
Ref-Lig-5	0.0380	48.57	
	Mass^2 at the end of recording		
Ac-Lig-1	0.0286	63.39	60.46 ± 2.28
Ac-Lig-2	0.0337	60.89	
Ac-Lig-3	0.0325	61.46	
Ac-Lig-4	0.0413	57.41	
Ac-Lig-5	0.0374	59.17	
	Mass^2 at the end of recording		
P-Lig-1	0.378	–	–
P-Lig-2	0.403	–	
P-Lig-3	0.430	–	
P-Lig-4	0.418	–	
P-Lig-5	0.446	–	

reason is probably that a change in morphology occurs when the liquid is in contact with the lignin and then Washburn hypotheses (with a constant c $\bar{r}$) are not valid [43,58]. This interaction between lignin and ethylene glycol was observed in the literature [61] and here, it causes a slight decrease of mass before achieving the equilibrium. Further studies have to be focused on this phenomenon. It is interesting to note that the saturation of medium was never achieved with the ethylene glycol and the liquid reached different heights depending on the lignin. Using the Jurin approach, the apparent equilibrium contact angles were then found. The results are presented in Table 8. The highest contact angle was found for the Ac-Lig, for which the equilibrium mass was the lowest. Conversely, the lowest contact angle was found for the P-lig, for which the liquid quasi-totally wetted the powder (a small quantity of dry powders was observed at the top of the sample).

PLA is obtained from the polycondensation of lactic acid. Fig. 10 shows wicking curves obtained for all lignins with lactic acid and photos of one sample per lignin after the test. It is possible to observe that the wicking kinetics were significantly different for the P-Lig compared to the Ref-Lig and the Ac-Lig. The Ref-Lig and the Ac-Lig seemed to show a faster wicking, but the liquid did not reach a high equilibrium height. On the contrary, for the P-Lig a very slow wicking with a linear trend occurred (a fit using the Washburn equation up to 3000 s was possible). In this case the lactic acid reached the top of sample at 4500 s with a complete wetting of the powder. According to the Jurin approach, the equilibrium squared mass was used to determine the equilibrium contact angle for each lignin, as shown in Table 9. According to these observations, the equilibrium contact angle with lactic acid was 46.95 ± 2.66 for the Ref-Lig and 60.46 ± 2.28 for the Ac-Lig, while for the P-Lig cosines slightly superiors or equals to 1 were found suggesting that an angle of 0° can be considered. All equilibrium contact angles obtained applying the Jurin approach were finally used to determine the surface energy and the dispersive and polar components of lignins.

3.1.2. *Surface energy determination*

The surface energy and dispersive and polar components determination of lignins is possible using the Owens-Wendt equation and apparent equilibrium contact angles obtained using the modified Jurin

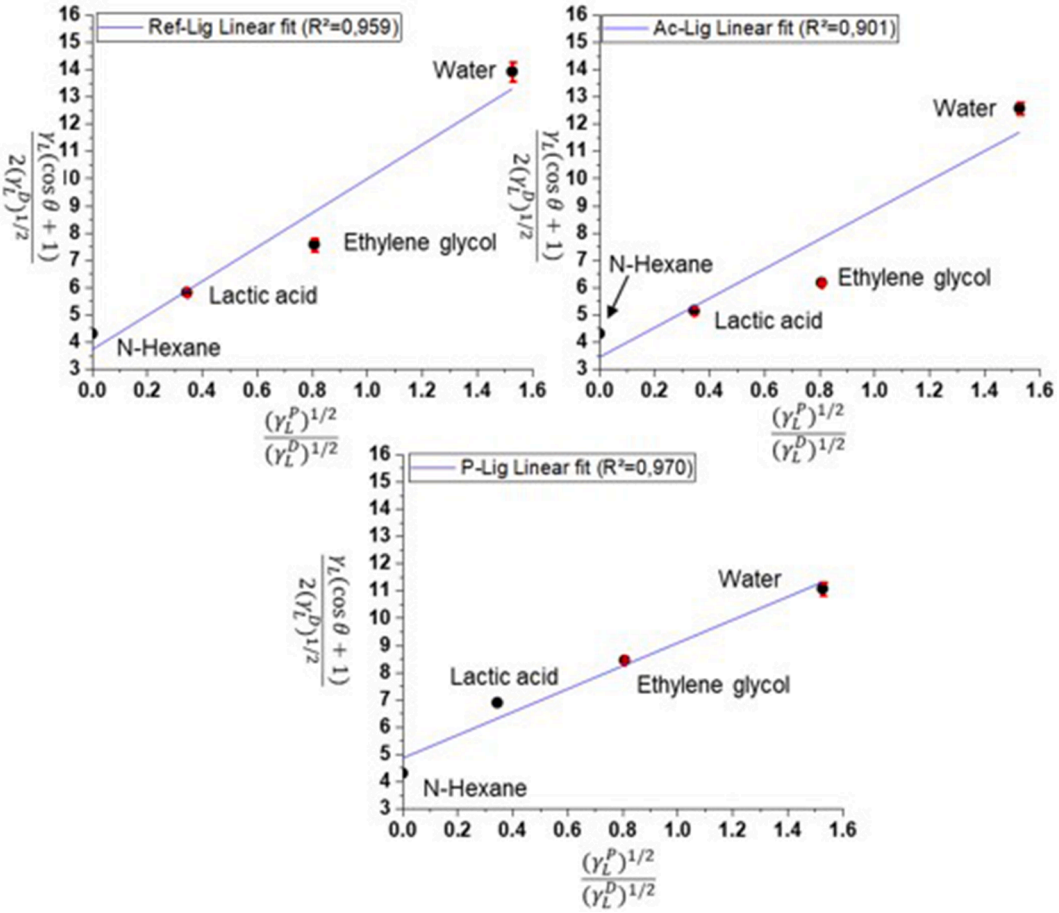

Fig. 11. Owens-Wendt linear fit using apparent equilibrium contact angles for Ref-Lig, Ac-Lig and P-Lig.

Table 10
Surface energy and components of the different lignins.

	Ref-Lig	Ac-Lig	P-Lig
γ_s^d (mN/m)	13.60 ± 0.18	11.64 ± 0.14	23.31 ± 0.34
γ_s^p (mN/m)	39.25 ± 2.85	29.17 ± 1.36	17.88 ± 1.42
γ_s (mN/m)	52.85 ± 3.03	40.81 ± 1. 50	41.19 ± 1.76

approach for porous media. Fig. 11 shows the linear regressions obtained using the Eq. (8) for the Ref-Lig, Ac-Lig and P-Lig. n-hexane is added as totally wetting liquid with an angle of 0°. It is possible to observe that the coefficient of determination (R^2) was quite high for all lignins (superior to 0.9). The surface energy and the dispersive and polar components obtained from fits are presented in Table 10.

Ref-Lig was found to have the highest surface energy (52.85 ± 3.03 mN/m) with a very high polar component (39.25 ± 2.85). In the literature, Notley et al. [62] found a quite similar surface energy ($\gamma s = 57.1$ mN/m) for a kraft lignin film using contact angles determined with a goniometer. Even if the two surface energy determination methods are different, the surface energies were close. However, the dispersive and polar components were not similar. The Ref-Lig is more polar, probably due to the OH and the Na + content. The Ac-Lig ($\gamma s = 40.81 \pm 1.50$ mN/m) and the P-Lig ($\gamma s = 41.19 \pm 1.76$ mN/m) have a lower surface energy with a widely reduced polar component. This is consistent with the fact that the chemical treatments removed a part of Na and grafting new functional groups on hydroxyl sites. Due to the effectiveness of treatments, the lignin clearly lost a large part of polar components. Reducing the polarity of lignin should have a beneficial effect on the adhesion with PLA that is a hydrophobic matrix [63]. P-Lig showed the lowest polar component (17.88 ± 1.42 mN/m) and, in addition, an increase of the dispersive component compared to Ref-Lig and Ac-Lig. This is due to the addition of phosphorus, which has a heavier electron cloud and facilitates instantaneous dipolar moments formation [64]. Finally, these results seem to be reliable and in agreement with results of other lignin characterizations. This proves that the modified Jurin approach coupled to an adapted experimental procedure for powders and porous media can be an effective and simple solution to determine suitable surface energy of these materials. Another interesting result is that the phosphorylation, known to be efficient for improving thermal stability of composites [51,60,65], could be also promising to improve the adhesion at the lignin/PLA interface compared to the acetylation, which is already known as an efficient treatment for this aim. Knowing filler surface energy components is also relevant to determine the work of adhesion between the filler and the matrix [38,67]. For PLA matrix, surface tension components should be determined at the molten state. However, as a first approximation, lactic acid dispersive and polar components could be used to calculate the work of adhesion.

3.1.3. *PLA/lignin interface observation*

The untreated and treated lignins were incorporated in PLA in order to observe the effect of the treatment on the adhesion at the interface between PLA and lignin. Fig. 12 shows SEM images of cryo-ultramicrotomed surfaces of biocomposites with Ref-Lig, Ac-Lig and P-Lig.

On sample A, spherical lignin particles dispersed in the PLA matrix can be easily identified. Despite the high pressure, high temperature and the high shear rate imposed by the process, the particle shapes appeared unmodified and well dispersed into the polymer. However, the presence of gaps at the lignin/PLA interface indicates a poor interfacial adhesion due to the poor compatibility between the hydrophilic lignin and the hydrophobic PLA [66,67]. On the contrary, the SEM image of sample B shows a good adhesion between PLA and acetylated lignin. Ac-Lig is not removed from the matrix and the presence of "scratches" on lignin are due to the diamond knife of cryomicrotome and prove that the lignin

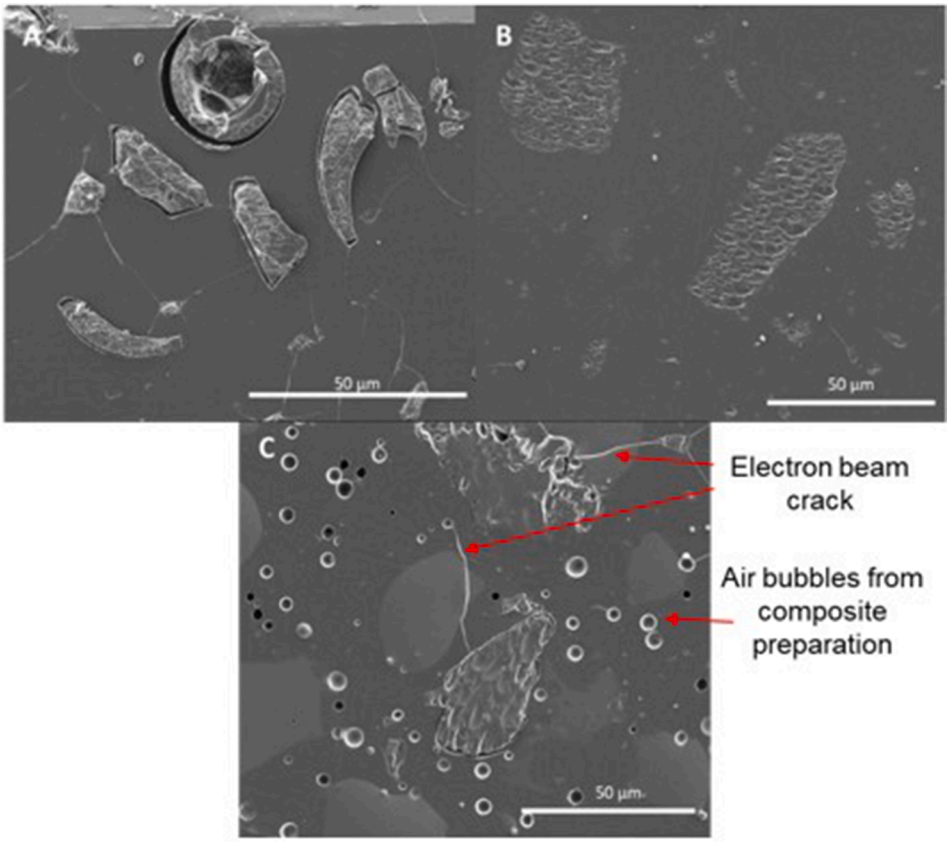

Fig. 12. SEM pictures of sample A, B and C.

particles did not move. Similar results are observed for PLA/P-Lig biocomposite, indicating a good adhesion at the interface between fillers and matrix. Further studies will be carried out on the mechanical behavior of biocomposites with untreated and treated lignins.

4. Conclusion

As a conclusion of this work, lignin was successfully treated by two different procedures: the acetylation and the phosphorylation. Lignin modifications due to both treatments were identified by FTIR, SEM-EDX and ICP characterizations. The thermal stability of lignins was also studied by TGA. Phosphorylation did not affect the thermal stability of the lignin in contrast with the acetylation that showed the lowest residual mass. To determine equilibrium contact angles and obtain surface energy components of untreated and treated lignins, an adapted experimental procedure coupled to an original Jurin approach for porous materials was set. Capillary wicking tests with different liquids were carried out on different lignins. The proposed method using the new Jurin approach was compared to the Washburn approach for porous media. Results showed that the Washburn theory had some limits for the application to these materials, since some hypotheses were not respected or no longer valid (typically the non-linearity of wicking curves for which apparent advancing contact angles could not be obtained). On the contrary, the new proposed method was in all cases applicable and gave results of apparent equilibrium contact angles for all lignins with all liquids. These values were used to obtain the surface energy and dispersive and polar components of different lignins according to the Owens-Wendt equation. Surface energy results were found to be consistent with the literature and with lignins characterizations. This proved that the proposed method could be an effective and simple solution to determine suitable surface energy of powders and porous media. In further studies, the approach will be applied to other types of materials and at different scales in order to verify its larger or limited validity. Results for untreated and treated lignin surface energy were relevant, showing that the phosphorylation, known to improve the thermal behavior of lignin/PLA composites, also reduced the polarity of lignin. Moreover, the treatment increased the dispersive component of lignin compared to the acetylation. Then it could be potentially more effective to enhance the adhesion with the PLA matrix. Further studies about the enhancement of interface adhesion and the mechanical behavior of this interface represent the perspectives of this work.

Funding

Occitanie Region.

CRediT authorship contribution statement

Valentin Carretier: Writing – original draft, Methodology, Investigation, Formal analysis. **Monica Francesca Pucci:** Conceptualization, Validation, Methodology, Investigation, Formal analysis, Writing – review & editing. **Clément Lacoste:** Conceptualization, Methodology. **Arnaud Regazzi:** Conceptualization, Methodology. **José-Marie Lopez-Cuesta:** Conceptualization, Methodology, Funding acquisition, Supervision, Writing – review & editing.

Declaration of Competing Interest

The authors declare that they have no known competing financial interests or personal relationships that could have appeared to influence the work reported in this paper.

Acknowledgments

The authors thank J.C. Roux of C2MA for his help to conduct the SEM characterizations.

References

[1] M. Murariu, P. Dubois, PLA composites: From production to properties, Adv. Drug Deliv. Rev. 107 (2016) 17–46.
[2] R. Auras, B. Harte, S. Selke, An overview of polylactides as packaging materials, Macromol. Biosci. 4 (9) (2004) 835–864.
[3] M. Jamshidian, E.A. Tehrany, M. Imran, M. Jacquot, S. Desobry, Poly-lactic acid: production, applications, nanocomposites, and release studies, Compr. Rev. Food Sci. Food Saf. 9 (5) (Aug. 2010) 552–571.
[4] D.-Y. Wang, A. Leuteritz, Y.-Z. Wang, U. Wagenknecht, G. Heinrich, Preparation and burning behaviors of flame retarding biodegradable poly(lactic acid) nanocomposite based on zinc aluminum layered double hydroxide, Polym. Degrad. Stab. 95 (12) (Dec. 2010) 2474–2480.
[5] E.O. Cisneros-López, et al., Recycled poly(lactic acid)–based 3D printed sustainable biocomposites: a comparative study with injection molding, Mater. Today Sustain. 7–8 (Mar. 2020), 100027.
[6] F.H.M. Graichen, W.J. Grigsby, S.J. Hill, L.G. Raymond, M. Sanglard, D.A. Smith, G.J. Thorlby, K.M. Torr, J.M. Warnes, Yes, we can make money out of lignin and other bio-based resources, Ind. Crops Prod. 106 (2017) 74–85.
[7] S. Beisl, A. Friedl, A. Miltner, Lignin from micro- to nanosize: applications, Int. J. Mol. Sci. 18 (11) (Nov. 2017) 2367.
[8] E. Windeisen, G. Wegener, Lignin as building unit for polymers, in: M. Moeller, K. Matyjaszewski (Eds.), Polymer Science: A Comprehensive Reference, vol. 10, Elsevier, Amsterdam, Netherlands, 2012, pp. 255–265.
[9] A. Tribot, G. Amer, M. Abdou Alio, H. de Baynast, C. Delattre, A. Pons, J.-D. Mathias, J.-M. Callois, C. Vial, P. Michaud, C.-G. Dussap, Wood-lignin: Supply, extraction processes and use as bio-based material, Eur. Polym. J. 112 (2019) 228–240.
[10] A. Duval, F. Vilaplana, C. Crestini, M. Lawoko, Solvent screening for the fractionation of industrial kraft lignin, Holzforschung 70 (1) (2016) 11–20.
[11] C. Chio, M. Sain, W. Qin, Lignin utilization: A review of lignin depolymerization from various aspects, Renew. Sustain. Energy Rev. 107 (February) (Jun. 2019) 232–249.
[12] S. Laurichesse, L. Avérous, Chemical modification of lignins: Towards biobased polymers, Prog. Polym. Sci. 39 (7) (Jul. 2014) 1266–1290.
[13] Y.-L. Chung, et al., A renewable lignin-lactide copolymer and application in biobased composites, ACS Sustain. Chem. Eng. 1 (10) (Oct. 2013) 1231–1238.
[14] H. Sadeghifar, A. Ragauskas, Lignin as a UV Light Blocker—A Review, Polymers (Basel) 12 (5) (May 2020) 1134.
[15] Y. Qian, X. Qiu, S. Zhu, Sunscreen performance of lignin from different technical resources and their general synergistic effect with synthetic sunscreens, ACS Sustain. Chem. Eng. 4 (7) (2016) 4029–4035.
[16] M. Zimniewska, R. Kozłowski, J. Batog, Nanolignin modified linen fabric as a multifunctional product, Mol. Cryst. Liq. Cryst. 484 (1) (2008) 43/[409]–50/[416].
[17] T.V. Lourençon, et al., Antioxidant, antibacterial and antitumoural activities of kraft lignin from hardwood fractionated by acid precipitation, Int. J. Biol. Macromol. 166 (2021) 1535–1542.
[18] M.H. Sipponen, H. Lange, C. Crestini, A. Henn, M. Österberg, Lignin for nano- and microscaled carrier systems: applications, trends, and challenges, ChemSusChem 12 (10) (2019) 2039–2054.
[19] V. Ugartondo, M. Mitjans, M.P. Vinardell, Comparative antioxidant and cytotoxic effects of lignins from different sources, Bioresour. Technol. 99 (14) (2008) 6683–6687.
[20] Q.i. Lu, M. Zhu, Y. Zu, W. Liu, L. Yang, Y. Zhang, X. Zhao, X. Zhang, X. Zhang, W. Li, Comparative antioxidant activity of nanoscale lignin prepared by a supercritical antisolvent (SAS) process with non-nanoscale lignin, Food Chem. 135 (1) (2012) 63–67.
[21] L. Dumazert, D. Rasselet, B.o. Pang, B. Gallard, S. Kennouche, J.-M. Lopez-Cuesta, Thermal stability and fire reaction of poly(butylene succinate) nanocomposites using natural clays and FR additives, Polym. Adv. Technol. 29 (1) (2018) 69–83.
[22] V. Carretier, J. Delcroix, M.F. Pucci, P. Rublon, J.-M. Lopez-Cuesta, Influence of sepiolite and lignin as potential synergists on flame retardant systems in polylactide (PLA) and polyurethane elastomer (PUE), Materials (Basel) 13 (11) (May 2020) 2450.
[23] A. Cayla, F. Rault, S. Giraud, F. Salaün, R. Sonnier, L. Dumazert, Influence of ammonium polyphosphate/lignin ratio on thermal and fire behavior of biobased thermoplastic: The case of Polyamide 11, Materials (Basel) 12(7), 2019.
[24] C. Réti, M. Casetta, S. Duquesne, S. Bourbigot, R. Delobel, Flammability properties of intumescent PLA including starch and lignin, Polym. Adv. Technol. 19 (6) (2008) 628–635.
[25] R. Zhang, X. Xiao, Q. Tai, H. Huang, J. Yang, Y. Hu, Preparation of lignin-silica hybrids and its application in intumescent flame-retardant poly(lactic acid) system, High Perform. Polym. 24 (8) (2012) 738–746.
[26] A. Cayla, F. Rault, S. Giraud, F. Salaün, V. Fierro, A. Celzard, PLA with intumescent system containing lignin and ammonium polyphosphate for flame retardant textile, Polymers (Basel) 8 (9) (Sep. 2016) 331.
[27] A. Duval, M. Lawoko, A review on lignin-based polymeric, micro- and nano-structured materials, React. Funct. Polym. 85 (2014) 78–96.
[28] C. Jiang, H. He, H. Jiang, L. Ma, D.M. Jia, Nano-lignin filled natural rubber composites: Preparation and characterization, Express Polym. Lett. 7 (5) (2013) 480–493.
[29] J. Kong, et al., Oxidation of Organosolv Lignin in a Novel Surfactant-free Microemulsion Reactor, Bioresour. Technol. 321(December 2020) (2020) p. 124466.

[30] N. Alwadani, P. Fatehi, Synthetic and lignin-based surfactants: Challenges and opportunities, Carbon Resour. Convers. 1 (2) (2018) 126–138.
[31] B.V.K.J. Schmidt, V. Molinari, D. Esposito, K. Tauer, M. Antonietti, Lignin-based polymeric surfactants for emulsion polymerization, Polymer (Guildf) 112 (2017) 418–426.
[32] J. Guo, X. Chen, J. Wang, Y. He, H. Xie, Q. Zheng, The influence of compatibility on the structure and properties of PLA/lignin biocomposites by chemical modification, Polymers (Basel). 12(1) (2020).
[33] L. Costes, F. Laoutid, M. Aguedo, A. Richel, S. Brohez, C. Delvosalle, P. Dubois, Phosphorus and nitrogen derivatization as efficient route for improvement of lignin flame retardant action in PLA, Eur. Polym. J. 84 (2016) 652–667.
[34] P. Figueiredo, K. Lintinen, J.T. Hirvonen, M.A. Kostiainen, H.A. Santos, Properties and chemical modifications of lignin: Towards lignin-based nanomaterials for biomedical applications, Prog. Mater. Sci. 93 (2018) 233–269.
[35] S.C. Fox, A.G. Mcdonald, Chemical and thermal characterization of three industrial lignins and their corresponding lignin esters, BioResources 5 (2) (2010) 990–1009.
[36] Y. Matsushita, Conversion of technical lignins to functional materials with retained polymeric properties, J. Wood Sci. 61 (3) (2015) 230–250.
[37] O. Gordobil, R. Delucis, I. Egüés, J. Labidi, Kraft lignin as filler in PLA to improve ductility and thermal properties, Ind. Crops Prod. 72 (2015) 46–53.
[38] L. Jeantet, A. Regazzi, A. Taguet, M.F. Pucci, A.-S. Caro, J.-C. Quantin, Biopolymer blends for mechanical property gradient 3d printed parts, Express Polym. Lett. 15 (2) (2021) 137–152.
[39] S. Kirdponpattara, M. Phisalaphong, B. min Z. Newby, Applicability of Washburn capillary rise for determining contact angles of powders/porous materials, J. Colloid Interface Sci. 397 (2013) pp. 169–176.
[40] M. Brugnara, C. Della Volpe, D. Maniglio, A. Penati, Wettability of porous materials, II: Can we obtain the contact angle from the Washburn equation? Contact Angle, Wettability Adhes. 4 (January) (2020) 155–176.
[41] S.B. Lee, P. Luner, The wetting and interfacial properties of lignin, Tappi 55 (1) (1972) 161–1121.
[42] R. Masoodi, E. Languri, A. Ostadhossein, Dynamics of liquid rise in a vertical capillary tube, J. Colloid Interface Sci. 389 (1) (2013) 268–272.
[43] M.F. Pucci, P.-J. Liotier, S. Drapier, Capillary wicking in flax fabrics - Effects of swelling in water, Colloids Surfaces A Physicochem. Eng. Asp. 498 (2016) 176–184.
[44] M.F. Pucci, P.-J. Liotier, S. Drapier, Capillary wicking in a fibrous reinforcement - Orthotropic issues to determine the capillary pressure components, Compos. Part A Appl. Sci. Manuf. 77 (2015) 133–141.
[45] B. Neirinck, D. Soccol, J. Fransaer, O.V.D. Biest, J. Vleugels, Influence of short chain organic acids and bases on the wetting properties and surface energy of submicrometer ceramic powders, J. Colloid Interface Sci. 348 (2) (2010) 654–660.
[46] K.-C. Chu, H.-K. Tsao, Y.-J. Sheng, Penetration dynamics through nanometer-scale hydrophilic capillaries: Beyond Washburn's equation and extended menisci, J. Colloid Interface Sci. 538 (2019) 340–348.
[47] J. Shang, M. Flury, J.B. Harsh, R.L. Zollars, Comparison of different methods to measure contact angles of soil colloids, J. Colloid Interface Sci. 328 (2) (2008) 299–307.
[48] J. Jiang, Q. Guo, B. Wang, L. Zhou, C. Xu, C. Deng, X. Yao, Y. Su, J. Wang, Research on variation of static contact angle in incomplete wetting system and modeling method, Colloids Surfaces A Physicochem. Eng. Asp. 504 (2016) 400–406.
[49] W. Wu, R.F.J. Giese, C.J. van Oss, Evaluation of the Lifshitz-van der Waals/Acid-Base Approach To Determine Surface Tension Components, Langmuir 11 (1) (1995) 379–382.
[50] M.F. Pucci, P.-J. Liotier, S. Drapier, Tensiometric method to reliably assess wetting properties of single fibers with resins: Validation on cellulosic reinforcements for composites, Colloids Surfaces A Physicochem. Eng. Asp. 512 (2017) 26–33.
[51] Y. Guo, C. Cheng, T. Huo, Y. Ren, X. Liu, Highly effective flame retardant lignin/polyacrylonitrile composite prepared via solution blending and phosphorylation, Polym. Degrad. Stab. 181 (2020), 109362.
[52] W. Ji, et al., The preparation of starch derivatives reacted with urea-phosphoric acid and effects on fire performance of expandable polystyrene foams, Carbohydr. Polym. 233 (January) (2020), 115841.
[53] C. Gao, L. Zhou, S. Yao, C. Qin, P. Fatehi, Phosphorylated kraft lignin with improved thermal stability, Int. J. Biol. Macromol. 162 (Nov. 2020) 1642–1652.
[54] E.W. Washburn, The Dynamics of Capillary Flow, Phys. Rev. 17 (3) (1921) 273–283.
[55] S. Liu, S. Li, J. Liu, Jurin's law revisited: Exact meniscus shape and column height, Eur. Phys. J. E 41 (3) (2018) 1–7.
[56] J. Liu, S. Li, Capillarity-driven migration of small objects: A critical review, Eur. Phys. J. E 42 (1) (2019) 1–23.
[57] W. Garat, et al., Surface energy determination of fibres for Liquid Composite Moulding processes: Method to estimate equilibrium contact angles from static and quasi-static data, Colloids Surfaces A Physicochem. Eng. Asp. 611(July 2020) (2021) p. 125787.
[58] H.N. Vo, M.F. Pucci, S. Corn, N. Le Moigne, W. Garat, S. Drapier, P.J. Liotier, Capillary wicking in bio-based reinforcements undergoing swelling – Dual scale consideration of porous medium, Compos. Part A Appl. Sci. Manuf. 134 (2020) 105893, https://doi.org/10.1016/j.compositesa:2020.105893.
[59] O. Gordobil, I. Egüés, R. Llano-Ponte, J. Labidi, Physicochemical properties of PLA lignin blends, Polym. Degrad. Stab. 108 (2014) 330–338.
[60] B. Prieur, et al., Phosphorylation of lignin: characterization and investigation of the thermal decomposition, RSC Adv. 7 (27) (2017) 16866–16877.
[61] L. Mu, Y. Shi, H. Wang, J. Zhu, Lignin in Ethylene Glycol and Poly(ethylene glycol): Fortified Lubricants with Internal Hydrogen Bonding, ACS Sustain. Chem. Eng. 4 (3) (2016) 1840–1849.
[62] S.M. Notley, M. Norgren, Surface energy and wettability of spin-coated thin films of lignin isolated from wood, Langmuir 26 (8) (2010) 5484–5490.
[63] M.A. Elsawy, K.H. Kim, J.W. Park, A. Deep, Hydrolytic degradation of polylactic acid (PLA) and its composites, Renew. Sustain. Energy Rev. 79(June 2016) (2017) pp. 1346–1352.
[64] J.-M. Douillard, F. Salles, M. Henry, H. Malandrini, F. Clauss, Surface energy of talc and chlorite: Comparison between electronegativity calculation and immersion results, J. Colloid Interface Sci. 305 (2) (2007) 352–360.
[65] B. Prieur, M. Meub, M. Wittemann, R. Klein, S. Bellayer, G. Fontaine, S. Bourbigot, Phosphorylation of lignin to flame retard acrylonitrile butadiene styrene (ABS), Polym. Degrad. Stab. 127 (2016) 32–43.
[66] D. Kun, B. Pukánszky, Polymer/lignin blends: Interactions, properties, applications, Eur. Polym. J. 93 (April) (2017) 618–641.
[67] C.A. Fuentes, Y. Zhang, H. Guo, W. Woigk, K. Masania, C. Dransfeld, J. De Coninck, C. Dupont-Gillain, D. Seveno, A.W. Van Vuure, Predicting the adhesion strength of thermoplastic/glass interfaces from wetting measurements, Colloids Surfaces A Physicochem. Eng. Asp. 558 (2018) 280–290.